Int. J. Electrochem. Sci., 10 **(2015)** 5465 - 5478

International Journal of
ELECTROCHEMICAL
SCIENCE
www.electrochemsci.org

Electrodeposition and Characterization of Zn-Ni-Mn Alloy from Sulfate Bath: Influence of Current Density

F. H. Assaf[1], *A. M. A. El-Seidy*[2,3], *M. M. Abou-Krisha*[1, 3,*] *and A. A. Eissa*[1]

[1]Faculty of Science, Chemistry Department, South Valley University, Qena, 83523, Egypt.
[2]Inorganic Chemistry Department, National Research Centre, P.O. 12622, Dokki, Giza, Egypt.
[3]College of Science, Chemistry Department, Al Imam Mohammad Ibn Saud Islamic University (IMSIU), Riyadh 11623, KSA.
[*]E-mail: m_abou_krisha@yahoo.com

Received: 26 March 2015 / *Accepted:* 15 April 2015 / *Published:* 27 May 2015

A sulfate bath was used to investigate the influence of current density on the electrodeposition behavior of Zn-Ni-Mn on steel. The presence of Zn^{2+} in the plating bath during Zn–Ni–Mn alloys codeposition is the cause of significant inhibition of Ni and Mn deposition. A transition current density was noticed above where in a transition from normal to anomalous deposition took place. At a higher current density, a uniform surface deposit of Zn–Ni–Mn was obtained. At lowest current densities, The deposits showed higher corrosion resistance because of normal deposition and for the highest studied current densities attributed to the thickness and the surface morphology. Cyclic voltammetry and galvanostatic techniques for electrodeposition were utilized in the investigation while linear polarization resistance and anodic linear sweeping voltammetry techniques were used for the corrosion study. The results revealed that the increase in current density favors the increase of Ni and Mn contents in the deposits. Zn-Ni-Mn alloys with higher Ni content showed higher resistance to corrosion and higher cathodic current efficiency.

Keywords: Electrodeposition; Anomalous codeposition; Surface morphology; Corrosion resistance; Ternary Zn-Ni-Mn alloy

1. INTRODUCTION

The use of coating as anticorrosive for metal substrates depends mainly on the sacrificial and barrier protection mechanisms. In industry the main demand is coating substances with the highest corrosion resistance and smallest thickness, which Zn coatings cannot provide, hence scientists replaced Zn coatings by Zn alloy coatings [1-5]. In electrodeposition the growth mechanism, morphology and micro-structural properties of the film is based on electrodeposition conditions such

as current density. The electrodeposition of Zn with Fe-group metals may be considered as anomalous codeposition because the less noble Zn deposits preferentially in most plating conditions, this was explained with different hypotheses [6, 7]. Zn-Ni alloys electrodeposited have greater corrosion protection, improved mechanical properties and better thermal stability than the corresponding bare zinc and other zinc alloy coatings [8]. Zn-Mn alloys electrodeposition are a growing interest because of their superior protective properties [9, 10]. A better mechanical properties were attended by decreasing the manganese content in coating for automotive applications as well as steel protection in different aggressive environments. It sensed that it will be important to accumulate the properties of Zn-Ni and Zn-Mn binary alloys in one alloy through the electrodeposition of Zn-Ni-Mn ternary alloy. The influence of current density on the alloys electrodeposition was studied by different researchers [11-14] but not with the present alloy. In this study, the composition, morphology and corrosion resistance of electrodeposited Zn-Ni-Mn films were investigated as a function of the current density values in the electrolyte. We have shown that the composition, grain size and morphology of the films were significantly affected by the current density.

2. EXPERIMENTAL

2.1 Reagents

The basic electrolyte chemical composition of Zn-Ni-Mn bath is Na_2SO_4 [0.20 M], H_3BO_3 [0.20M], H_2SO_4 [0.01 M], $MnSO_4$ [0.10 M], $NiSO_4$ [0.10 M] and $ZnSO_4$ [0.10 M]. The electrolytes and all used solutions were freshly prepared from Analar grade

2.2 Methods

All experiments were carried out in duplicated and the result reproducibility of these measurements was found to be acceptable. For a standard bath deposition, a series of experiments at different times were carried out and the relative standard deviation (RSD%) was found to be 4.3, 3.6 and 4.7% for the Zn, Ni and Mn contents in the deposit, respectively. Electrochemical measurements were performed using EG&G Potentiostate/Galvanostat model 273A controlled by a PC using 352 corrosion software. The electrochemical corrosion measurements of the coatings; polarization resistance (R_p), corrosion potential ($E_{corr.}$) and corrosion current density (i_{corr}) achieved and denoted (Table 1). The galvanostatic measurements were conducted by keeping the current density of cathodes constant (0.5 - 40 mA cm^{-2}, for 10 minutes). The chemical composition of Zn-Ni-Mn deposits were determined using atomic absorption spectroscopy (Thermo scientific, model ICE 3000 series AA spectrometer). These data were used to calculate the efficiency of the process. The deposited layer of Zn-Ni-Mn alloy was dissolved in 50.0 cm^3 of 20% HCl solution, and the suitable diluted solution was then analyzed to find out the Zn, Ni and Mn contents in the deposited alloy.

Table 1. Values of Zn, Ni and Mn mass, total mass, content% of Zn, Ni and Mn, current efficiencies of Zn-Ni-Mn deposits, thickness and electrochemical corrosion measurements of the deposits obtained galvanostatically at different cathodic current densities at 25.0 ^{o}C on steel substrate from a standard bath.

Parameter \ Current density (mA/cm^2)	1	3	5	10	20	30	40
Zn mass in the deposit × 10^{-4} / g	3.10	8.40	14.2	28.2	53.4	82.3	111
Ni mass in the deposit × 10^{-4} / g	0.30	0.47	0.97	2.30	7.4	11.7	18.8
Mn mass t in the deposit × 10^{-4} / g	0.07	0.20	0.35	0.72	1.86	3.14	4.92
The total mass of the deposit × 10^{-4} / g	3.47	9.07	15.5	31.2	62.7	97.1	134.7
Zn content / %	89.3	92.6	91.5	90.3	85.2	84.7	82.4
Ni content / %	8.7	5.2	6.3	7.4	11.8	12.1	13.9
Mn content / %	2.0	2.2	2.25	2.3	3.0	3.2	3.7
Zn-Ni-Mn alloy current efficiency ($e_{Zn-Ni-Mn}$) / %	86.5	75.1	77.2	77.8	78.5	81.2	84.8
the deposit Thickness / μm	0.24	0.63	1.07	2.2	4.26	6.6	9.1
Corrosion potential ($E_{corr.}$) / mV	-455	-993	-984	-924	-817	-731	-702
Corrosion current density ($i_{corr.}$) / μA cm^{-2}	8.4	52.0	47.6	39.9	31.7	26	21.6
Polarization resistance (R_p) / kΩ	15.5	3.8	4.2	4.8	5.9	7.9	9.3

The cathode current efficiencies of pure Zn, Ni and Mn were determined according to Faraday's laws is as detailed in Ref [15]. The X-ray diffraction patterns of the obtained deposits were recorded with a Brucker Axs-D8 Advance X-ray diffractometer using Cu-Kα radiation, to find the different deposited alloy phases. The surface morphology of the deposit is evaluated by using a scanning electron microscope, (JSM-5500 LV, SEM, JEOL, Japan). The Zn and Ni content in the deposit have been confirmed by EDS (Energy Dispersive X-ray Spectrometer) system with link Isis software and model 6587 An X-ray detector (OXFORD, UK). The thickness of the deposited alloy layer has been approximately estimated from the amount of deposit and the densities of Zn (d_{Zn}=7.14 g cm^{-3}), Ni (d_{Ni}=8.90 g cm^{-3}) and Mn (d_{Zn}=7.21 g cm^{-3}) [16,17] and confirmed by SEM (cross-section). The experiments have been done without cathode movement or solution agitation.

3. RESULTS AND DISCUSSION

3.1. Galvanostatic measurements

Current density is directly related to the economic efficiency and alloy properties, hence it is a very important variable in the electrodeposition process. Many factors affect the current density or cathodic potential such as chemical composition, appearance, corrosion resistance and quality of the alloys [16]. In order to monitor the potential with time, a galvanostatic curves are plotted in a static electrolyte under constant current densities for 10 minutes.

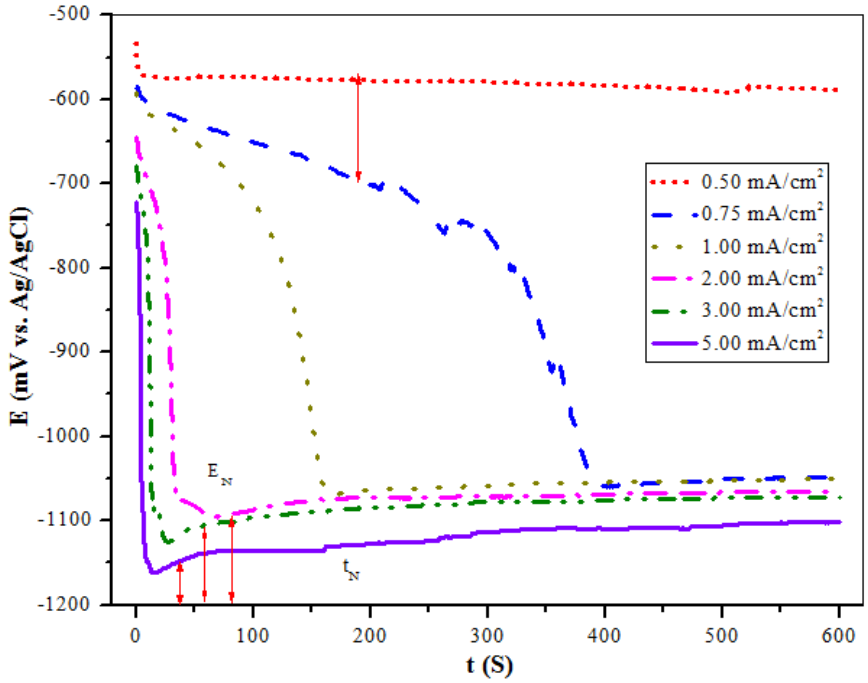

Figure 1. E - t curves for steel in a standard bath at 25.0 ^{o}C for 10 minutes at different low cathodic current densities.

Figure (1) shows the potential-time dependence for the electrodeposition of Zn-Ni-Mn alloys on steel rod at 0.5 to 5 mA cm^{-2} range cathodic current densities. During the first few seconds and at a current density of 0.5 mA cm^{-2}, the potential shifts rapidly to more negative values due to the nucleation process. As the time increases, the potential reaches a constant small value (-578 mV) of potential which indicates that only the nobler metal (Ni) is deposited at this current density. This indicates that at very low deposition current density, the deposit consists of a very nickel-enrich phase and the deposition takes place with very low overpotential. During the first 270 seconds and at a current density of 0.75 mA cm^{-2}, the potential increases gradually to more electronegative values till reaching a current density of -755 mV indicating obtaining nickel-enrich deposits (i.e., normal codeposition) where Ni needs low nucleation overpotential. During the next 120 seconds, the potential increases sharply till reaching the value of -1054 mV indicating the deposition of Zn and/or Mn. During the remaining time, the alloy grows at a constant potential value which is approximately -1054 mV. For the duration of the first 100 seconds at a current density of 1.0 mA cm^{-2}, the potential increases gradually to more electronegative values till reaching the value of -727 mV indicating obtaining nickel-enrich deposits because of the small negative value of potential. During the next 70 seconds, the potential increases sharply till reaching the value of -1069 mV indicating the deposition of Zn and/or Mn (i.e., anomalous codeposition). During the remaining time, the alloy grows at a fixed potential value which is about -1058 mV. Throughout the first few seconds at current densities of 2, 3 and 5 mA cm^{-2}, the potential shifts suddenly to more electronegative values indicating the nucleation process. As the time increases, the potential slightly move to more positive values, then the alloys grow at constant values of potentials. These constant values of potentials mean that the

composition of the deposited alloys remains unchanged during the growth process. It is very clear from the same figure that the nucleation time (t_N) reduces as the constant current density is shifted to more cathodic values meanwhile the nucleation potential (E_N) shifts to more electronegative values. This refers to that more overpotential is needed to create the initial nucleus as the deposition current density increases to more cathodic values.

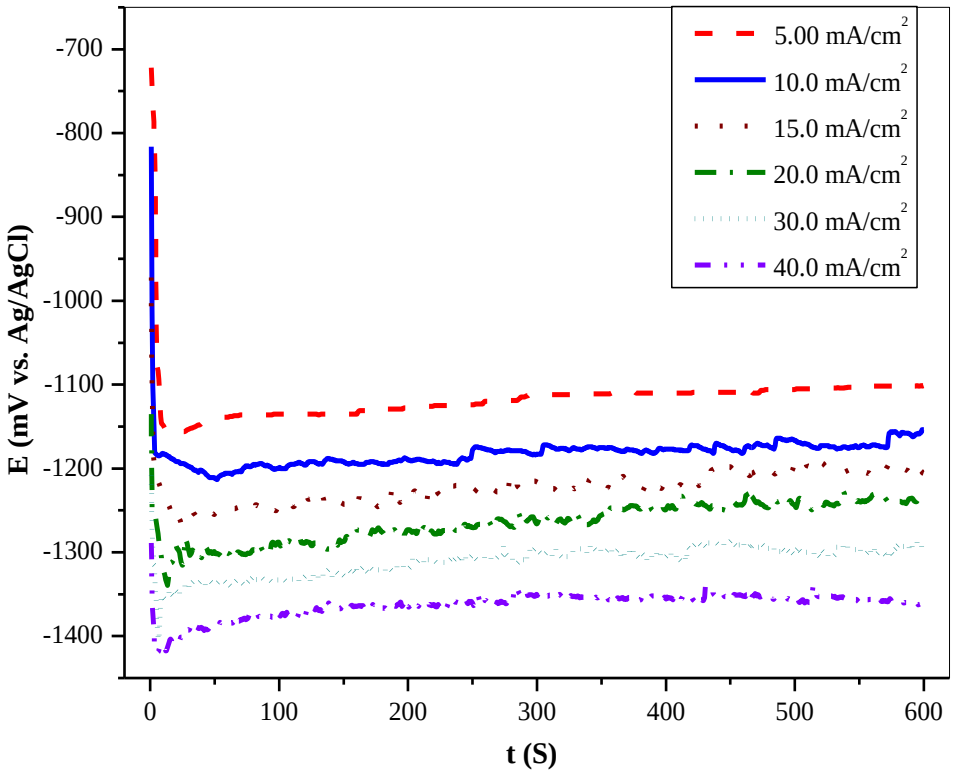

Figure 2. E - t curves for steel in a standard bath at 25.0 ^{o}C for 10 minutes at different high cathodic current densities.

Figure (2) shows the potential-time dependence for the electrodeposition of Zn-Ni-Mn alloys on steel rod at different high cathodic current densities ranging from 5 to 40 mA cm^{-2}. It is noticeable that all galvanostatic curves showed the same trend, the potential shifts rapidly to more cathodic values during the first few seconds as a result of the nucleation process in then reaches constant values at which the growth process of the deposits takes place. As the constant current density was shifted from 5 to 40 mA cm^{-2}, the galvanostatic curves shifted towards the cathodic direction which may be ascribed to the increase in the Zn and Mn amounts in the deposited alloy as a result of increasing the current density to more cathodic values. After the current density of 5 mA cm^{-2}, there are fluctuations of low frequency and magnitude in the galvanostatic curves which may be due to the increase in the hydrogen evolution reaction, the increase in the deposition rate and the increase in the nickel content in the deposited alloy which may lead to the formation of dendritic deposits at high cathodic current densities.

3.2. Galvanostatic cathodic polarization curve

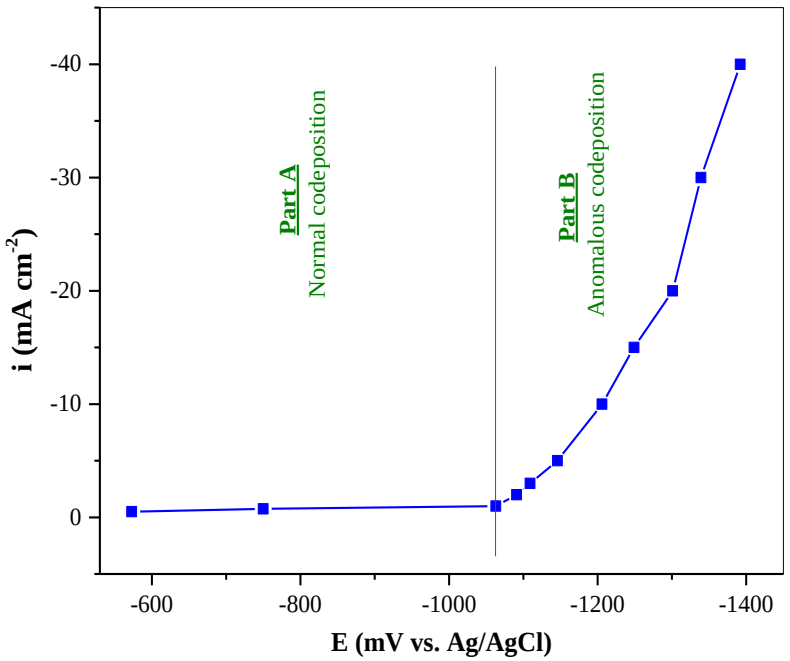

Figure 3. Galvanostatic cathodic polarization curve for Zn-Ni-Mn alloys obtained on steel rod from a standard bath at different cathodic current densities for 10 minutes at 25.0 ^{o}C.

Figure (3) shows the galvanostatic cathodic polarization curve for Zn-Ni-Mn alloys obtained at different deposition current densities ranging from 0.5 to 40 mA cm^{-2}. It is clear that the cathodic current density shifts slightly to more negative values till the potential of -1063 mV where normal deposition occurs, i.e., preferable deposition of Ni into the alloy (part A). After the potential of -1063 mV, the cathodic current density shifts rapidly to more negative values till the potential of -1392 mV where anomalous deposition occurs, i.e., preferable deposition of Zn and Mn into the alloy (part B). It is noticed that the normal deposition occurs at potentials which are positive to Zn deposition potential (E°_{Zn}= -1050 mV versus SCE) while anomalous deposition occurs at potentials which are negative to E°_{Zn}.

Hindrance in the discharge of nickel ions due to adsorption of zinc hydroxides may be One of the possible reasons for anomalous codeposition of zinc and nickel. The intense hydrogen production at near the cathode surface may cause these hydroxides to be formed as a result of electrolyte alkalization. However, it has been shown recently by measuring the pH_s values in the vicinity of the cathode surface in a plating solution of 0.5 M $NiSO_4$ + 0.5 M $ZnSO_4$, that the inhibition in the reduction of nickel ions does not result from the formation of zinc hydroxides because the pH_s values do not reach the values needed for hydroxide formation [17]. Accordingly, anomalous deposition of Zn and Ni in Zn-Ni-Mn alloy may be attributed to the high overpotential of nickel deposition on zinc substrate and peculiarities of the structure of the electric double layer containing the zinc ions together with the nickel ones. Due to

the zinc ion's higher surface activity, compared to nickel, the zinc ions replace the nickel ions in the dense part of double layer leading to an alloy enrichment with zinc [17]. When the zinc ions reduction rate decreases, a redistribution of ions concentration occurs in the dense part of the double layer leading to an increase in the nickel content at high cathodic current densities. This agrees well with the results of previous works [18]. Evidencing that the nickel content in the alloy grown in the acidic bath exhibits variations with current density. Therefore, the mechanism of nickel and zinc codeposition can be switched from anomalous to normal by changing the plating conditions (deposition potential or current density).

3.3. Anodic linear sweep voltammograms (ALSVs)

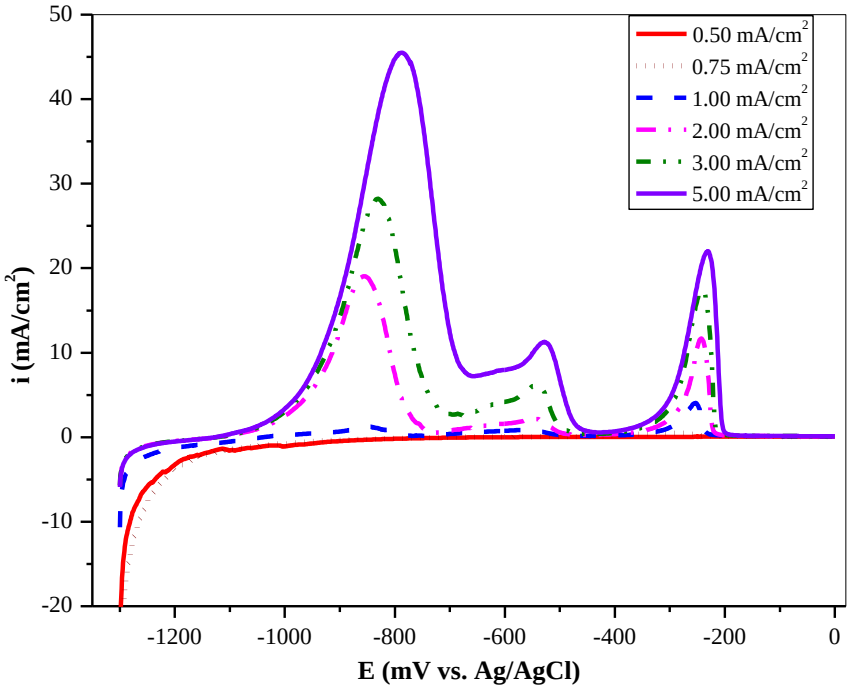

Figure 4. ALSVs for Zn-Ni-Mn alloys obtained on steel rod at 25.0 ^{o}C for 10 minutes at different low cathodic current densities from a standard bath, in 0.5 M Na_2SO_4 + 0.05 M EDTA at 5 mV/s and 25.0 ^{o}C.

Figure (4) shows the anodic linear sweep voltammograms (ALSVs) obtained during the dissolution of Zn-Ni-Mn alloys electrodeposited on steel rod at different low cathodic current densities ranging from 0.5 to 5 mA cm^{-2}. On the basis of the ALSVs, an identification of the phase structures present in the Zn-Ni-Mn alloys can be obtained. At a current density of 0.5 mA cm^{-2}, there are no anodic peaks indicating that the amount of Ni deposited is too small and is not sufficient to give apparently dissolution peak. At the current density of 0.75 mA cm^{-2}, there is only a very small anodic peak at -275 mV which is attributed to the dissolution of Ni previously deposited on the electrode surface. At a current density of 1.0 mA cm^{-2}, the dissolution of Zn-Ni-Mn alloy occurs under three

voltammetic peaks which are at potentials of -853, -558 and -253 mV. The first anodic peak is ascribed to the dissolution of Zn from pure zinc phase, the second one is attributed to the dissolution of Zn from γ-Ni_5Zn_{21} and/or δ-Ni_3Zn_{22} phases, and the third one is attributed to the dissolution of Ni from nickel phases. It is noticeable from the ALSV curve at 1.0 mA cm^{-2} that the height of the first two current peaks is low meanwhile the height of the third one is high indicating obtaining Ni-enrich deposits having good adhesion giving rise to normal codeposition.

At the current densities of 2, 3 and 5 mA cm^{-2}, the dissolution also occurs under three anodic current peaks. It is clear from the same figure that the height of the anodic peaks increases as a result of increasing the deposition current density to more cathodic values indicating the increase of the amount of alloy components and obtaining a thicker layer of the deposit on the substrate surface. Also, the dissolution peaks shift to more positive values giving rise to the improvement of the corrosion resistance properties of the deposits. As can be seen from the figure, there is a small shoulder at a current density of 3 mA cm^{-2} at -611 mV which may be attributed to the dissolution of Zn from a new zinc phase. This shoulder becomes at -595 at a current density of 5 mA cm^{-2} (i.e., at more noble potential).

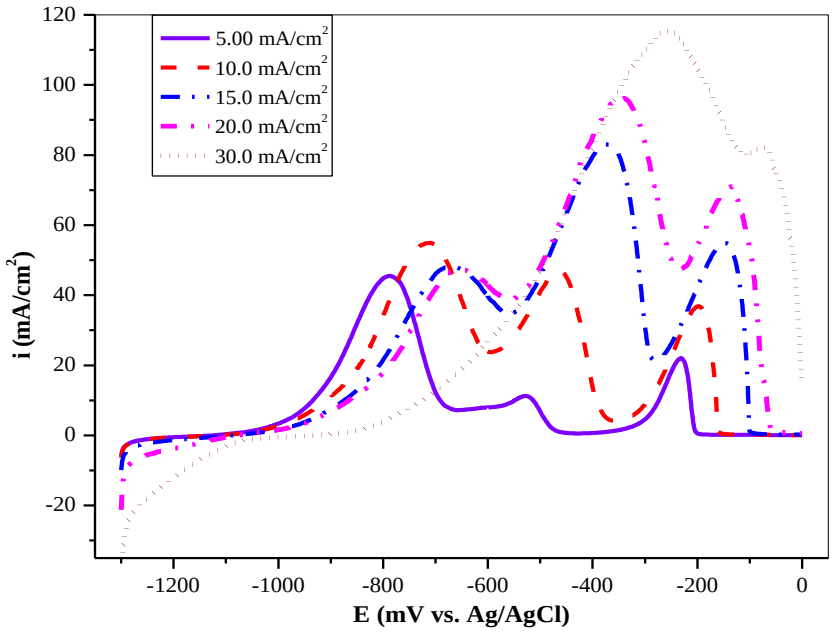

Figure 5. ALSVs for Zn-Ni-Mn alloys obtained on steel rod at 25.0 ^oC for 10 minutes at different high cathodic current densities from a standard bath, in 0.5 M Na_2SO_4 + 0.05 M EDTA at 5 mV/s and 25.0 ^oC.

Figure (5) shows the ALSVs obtained during the dissolution of Zn-Ni-Mn alloys electrodeposited on steel rod at different high cathodic current densities ranging from 5 to 30 mA cm^{-2}. It is obvious that when the deposition current density increases cathodically from 5 to 20 mA cm^{-2}, the height of the first anodic peak slightly increases meanwhile the height of the second and third anodic peaks rapidly increases. This indicates that the amount of pure zinc phase increases slowly while the amount of γ-Ni_5Zn_{21} and/or δ-Ni_3Zn_{22} phases increases rapidly as a result of the change in the current

density from 5 to 20 mA cm^{-2}. This is the reason responsible for shifting the anodic peaks towards the positive direction when the deposition current density is shifted towards the negative direction which leads to obtaining Zn-Ni-Mn alloys of good corrosion resistance properties at high cathodic current densities. The shoulder present at a current density of 3 and 5 mA cm^{-2} overlaps with the second anodic peak when the current density becomes more cathodic than 5 mA cm^{-2}.

The ALSV curve, at a current density of 30 mA cm^{-2}, has an abnormal dissolution peak shape where there is a very large decrease in the height of the first dissolution peak and a significant increase in the height of the second and third dissolution peaks. This indicates that there is a decrease in the content of the pure Zn phase and consequently an increase in the content of the γ-Ni_5Zn_{21} and/or δ-Ni_3Zn_{22} phases. In addition, increasing the content of the nobler phase of the alloy with increasing the current density towards the cathodic direction shifts the anodic peaks towards the positive direction, giving rise to the improvement of the corrosion resistance properties of the deposit. It is clear that the current density does not reach zero at the end of the oxidation process indicating that the deposit is not completely removed from the electrode surface as it has been recorded practically indicating obtaining an alloy of good adhesion and good corrosion resistance properties. It is noteworthy that Mn does not exhibit anodic peaks during the dissolution of the alloy. This may be ascribed to the low content of manganese in the deposited alloys with respect to the content of zinc and nickel, therefore the manganese anodic peak may overlap with the anodic peak of pure zinc phase. The low content of manganese is due to its high electronegative deposition potential with respect to the deposition potential of zinc and nickel.

3.4. Potentiodynamic polarization curves

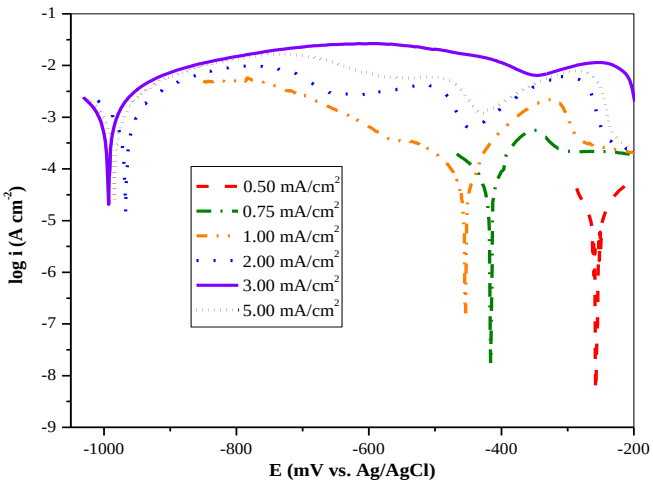

Figure 6. log i - E curves for Zn-Ni-Mn alloys obtained on steel rod at 25.0 ^{o}C for 10 minutes at different low cathodic current densities from a standard bath, in 0.05 M HCl at 5 mV/s and 25.0 ^{o}C.

Figure (6) exhibits the potentiodynamic polarization curves obtained from steel coated galvanostatically with Zn-Ni-Mn alloys electrodeposited at different low cathodic current densities ranging from 0.5 to 5 mA cm^{-2}. It is clear that the deposited alloys have more noble corrosion

potentials in the current density range from 0.5 to 1.0 mA cm^{-2}. This is because of obtaining Ni-enrich deposits, giving rise to normal electrodeposition. As the current density is shifted to more cathodic value from 1 to 2 mA cm^{-2}, the corrosion potential sharply shifts to more cathodic value from 455 to 967 mV then the it slightly increases to more cathodic values as the deposition current density is increased to more cathodic values from 2 to 5 mA cm^{-2}. This is due to the decrease in the nickel content as indicated from Table (1) where the nickel content decreases from 8.7% to 5.2% when the current density is shifted from 1 to 3 mA cm^{-2}.

Figure (7) shows the potentiodynamic polarization curves obtained from steel coated galvanostatically with Zn-Ni-Mn alloys electrodeposited at different high cathodic current densities ranging from 5 to 40 mA cm^{-2}. It is noticeable that the corrosion potential shifts generally to more positive values after the current density of 5 mA cm^{-2}. This may be attributed to the increase in the amount of deposited Ni in the alloy as a result of increasing the deposition current density to more negative values during the higher range. This interpretation agrees with the results obtained in Table (1) where the deposited alloys have high Ni content at high cathodic current densities. For example, the deposited alloy has 14.1% of Ni at a current density of 40 mA cm^{-2}. Similar results have been obtained during the dissolution of Zn-Ni alloys [19].

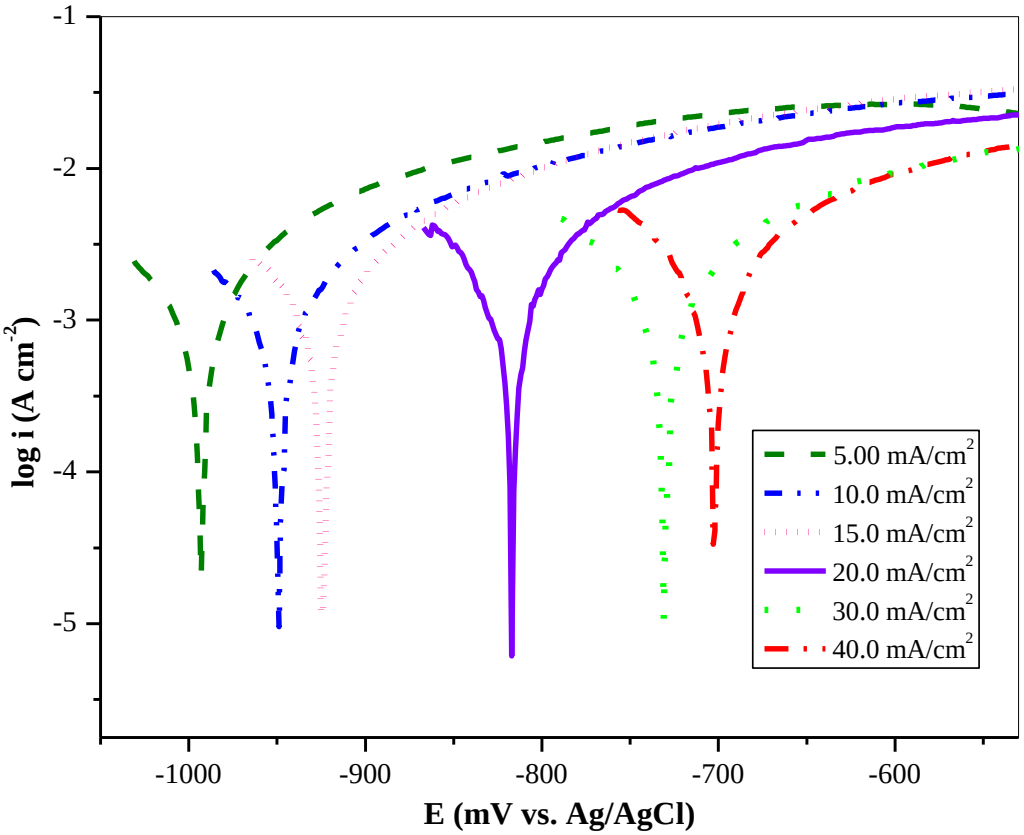

Figure 7. log i - E curves for Zn-Ni-Mn alloys obtained on steel rod at 25.0 ^{o}C for 10 minutes at different high cathodic current densities from a standard bath, in 0.05 M HCl at 5 mV/s and 25.0 ^{o}C.

3.5. Surface morphology

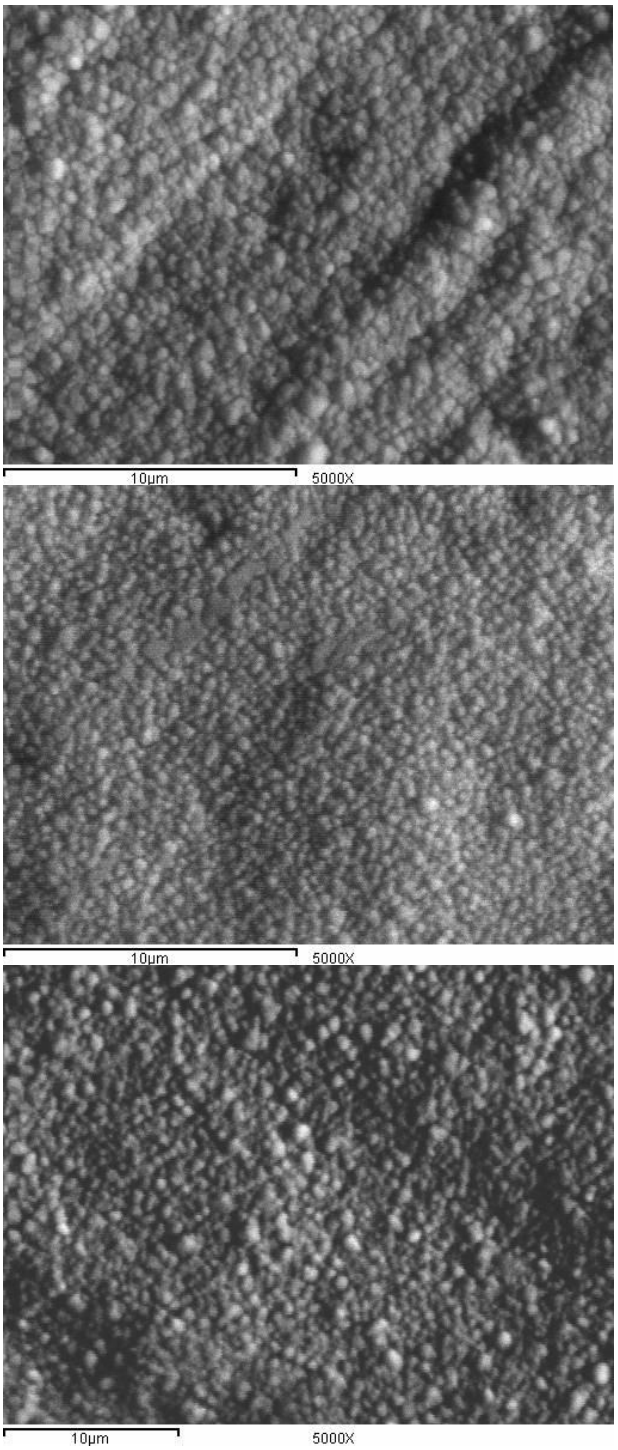

Figure 8. (a, b and c) SEM micrograph for Zn-Ni-Mn alloy electroplated on steel substrate of area 2 cm^2 at different cathodic current densities (a)10 mA/cm^2, (b)20 mA/cm^2 and (c)30 mA/cm^2 and 25.0 ^oC for 10 minutes from a standard bath.

Figures (8 a, b and c) show the scanning electron microscopy (SEM) micrographs for Zn-Ni-Mn alloys obtained on steel substrate at 25.0 ^oC at the current densities of 10, 20 and 30 mA/cm^2. It is clear that increasing the cathodic current density results in decreasing the grain size for the obtained

coatings. Consequently, the compactness, adherence and hardness increase with increasing the cathodic current density. The surface morphology of the coating at the current density of 30 mA/cm^2 has less uniformity and homogeneity which may be due to the increase in the deposition rate at high cathodic current densities. It is noticeable that the greatest homogeneity and uniformity, least grains size and highest crystallinity are at the current density of 20 mA/cm^2. Therefore, the most preferable surface morphology, appearance, hardness, compactness and adherence is at this current density. As can be seen from the figures, the three coatings completely cover the substrate and there are no cracks.

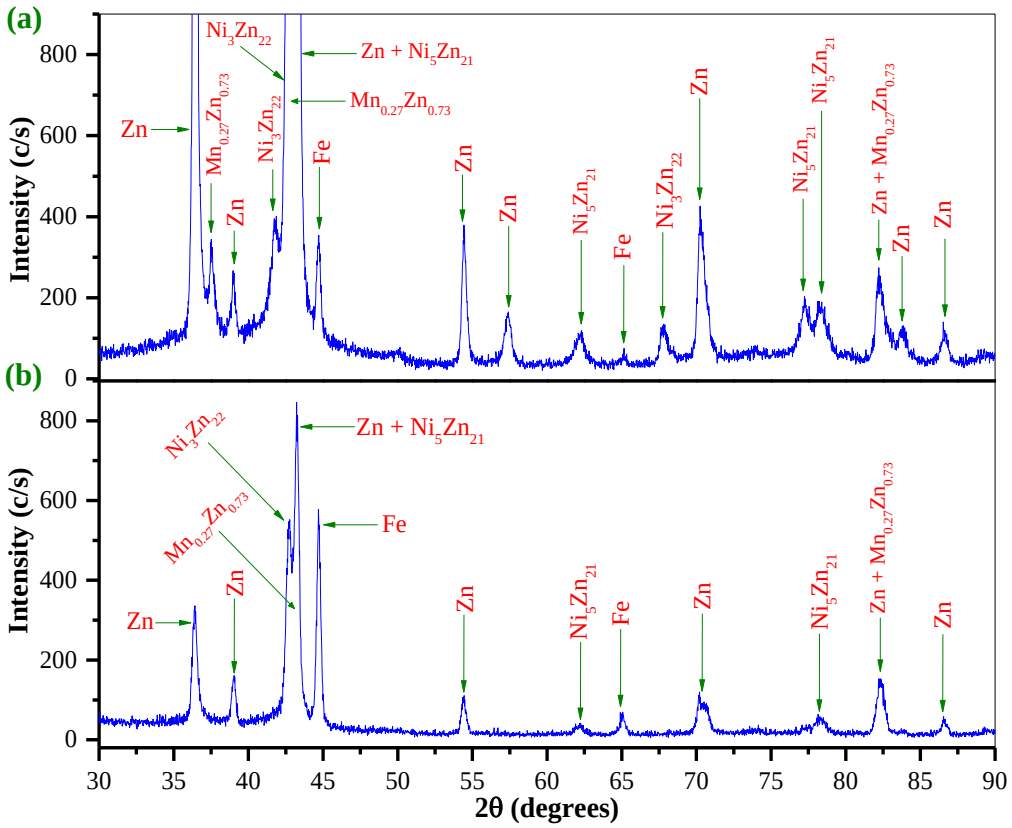

Figure 9. XRD peaks for Zn-Ni-Mn alloys electrodeposited on steel substrate of area 2 cm^2 at 25.0 ^{o}C for 10 minutes from a standard bath at: (a) 30 mA cm^{-2} and (b) -5 mA cm^{-2}.

Figure (9) exhibits the diffractograms of Zn-Ni-Mn alloys obtained at current densities of -5 and 30 mA/cm^2. It is clear that increasing the cathodic current density from 5 to 30 mA/cm^2 results in increment the intensity of all XRD peaks referring to the increment in the content of all phases. Moreover, some new peaks appear at the current density of 30 mA/cm^2 which are the peak at 2θ of 37.55 that corresponds to $Mn_{0.27}Zn_{0.73}$ phase, the peaks at 2θ of 41.75 and 67.8 that correspond to δ-Ni_3Zn_{22} phase and the peaks at 2θ of 57.3 and 83.7 that correspond to pure Zn phase. The intensity of the peaks that correlate to the substrate (at 2θ of 44.65 and 65.1) for the alloy obtained at 5 mA/cm^2 is higher than that for the alloy obtained at 30 mA/cm^2 indicating the higher thickness of the alloy electrodeposited at 30 mA/cm^2.

3.6. Electrochemical measurements and deposit composition

Table 1 illustrates the dependence of Zn-Ni-Mn alloy composition on the deposition current density. It is noticeable that the zinc content increases from 89.3% to 92.6% when the current density is shifted from 1 to 3 mA/cm^2 then decreases till reaching the value of 82.4% with shifting the current density to more negative values. The decrease in zinc content is replaced with an increase in nickel content at high cathodic current densities. The nickel content decreases from 8.7% to 5.2% when the current density is shifted from 1 to 3 mA/cm^2 then it increases till reaching the value of 13.9% with shifting the current density to more cathodic values. This increment may be ascribed to the lower overpotential of nickel deposition at higher cathodic current densities or to the decrease in zinc content at higher cathodic current densities. It has been reported elsewhere too that the increase in the applied current density results in an increase of the content of the nobler metal in the coating [20]. Similar results have been obtained during the electrodeposition of Zn-Ni-Fe [21] and Zn-Ni-Co [22] where increasing the current density to more cathodic values results in an increment of the nobler metals into the deposited alloy. The manganese content increases slowly from 2.0% to 3.7% with shifting the current density to more cathodic values. Similar results have been obtained during the electrodeposition of Mn-Co alloy [23] where increasing the cathodic current density results in an increment of manganese content into the deposited coating. It has been reported that the rate of Zn deposition is heavily influenced by mass-transport limitation at high applied cathodic current densities while the rate of Ni deposition is not [22].

The obtained results show that the dependence of the current efficiency of Zn, Ni and Mn metals and Zn-Ni-Mn alloy on the deposition current density. Both Zn^{2+} and Mn^{2+} have deposition potentials more negative than the potential for hydrogen evolution reaction, so H_2 evolution is always a parallel reaction during the alloy deposition. Consequently, the current efficiency of the alloy deposition will be always less than 100%. The thickness of the deposited alloy increases as the deposition current density increases to more cathodic values due to the increase in the content of the alloy components. Also, the electrochemical measurements all are in consitans with the thickness and the Ni content.

4. CONCLUSION

In the present research, Zn–Ni–Fe alloy deposits have been obtained from a sulfate bath at different current density values. The electrodeposition of Zn–Ni–Fe exhibited the phenomenon of anomalous type codeposition at the studied current densities from 3 to 40 mA cm^{-2}, but good surface appearance and acceptable corrosion resistance. According to current density the electrodeposition behavior of Zn–Ni–Fe alloy can be divided into two regions. In the first region and at low current density (0.5–1 mA cm^{-2}) a high corrosion resistance and normal codeposition was attained with high current efficiency, but in the second region and at high current density and at a low current efficiency a preferential deposition of less noble Zn (anomalous codeposition) proceeded. Accordingly, the best corrosion resistance to this type of alloy on steel substrate is obtained at current density in the range of 0.5–1 mA cm^{-2}.

The obtained results, indicated that Ni ions (or its monovalent intermediate) were adsorbed first, followed by the adsorption of Zn^{2+} and/or Mn^{2+} (or its monovalent intermediate), which inhibits the subsequent deposition of nickel ions (or its monovalent intermediate). This competition on occupying the active sites leads to the preferential deposition of Zn although it does not block the deposition of Ni and Mn completely.

References

1. C. Muller, M. Sarret and T. Andreu, *Electrochim. Acta* 48 (2003) 2397.
2. M. E. Bahrololoom, D. R. Gabe and G. D. Wilcox, *J. Electrochem. Soc*. 150 (2003) C144.
3. J. B. Bajat, V. B. Mišković-Stanković, M. D. Maksimović and D. M. Dražić, *Electrochim. Acta* 47 (2002) 4101.
4. H. Ashassi-Sorkhabi, A. Hagrah, N. Parvini-Ahmadi and J. Manzoori, *Surf. Coat. Technol*. 140 (2001) 278.
5. R. Ramanauskas, L. Gudavičiūtė, A. Kaliničenko and R. Juškėnas, *J. Solid State Electrochem*. 9 (2005) 900.
6. J. F. Huang and I. W.Sun, *J. Eelctrochem. Soc*. 151 (2004) C8.
7. T. Osaka, M. Takai, K. Hayashi, K. Ohashi, M. Saito and K. Yamada, *Nature* 392 (1998) 796.
8. C. Müller, M. Sarret, and M. Benballa, *Electrochim. Acta* 46 (2001) 2811.
9. C. Savall, C. Rebere, D. Sylla, M. Gadouleau, P. Refait and J. Creus, *Mater. Sci. Eng*. A 430 (2006) 165.
10. M. Bučko, J. Rogan, S. I. Stevanović, A. Perić-Grujić and J. B. Bajat, *Corros. Sci*. 53 (2011) 2861-2871.
11. K.S. Lew, M. Raja, S. Thanikaikarasan, T. Kim, Y.D. Kim and T. Mahalingam, *Mater. Chem. Phys*. 112 (2008) 249.
12. K. S. Lew, M. Raja, S. Thanikaikarasan, T. Kim, Y. D. Kim and T. Mahalingam, Courrier du Savoir - N° 18 (2014) 27.
13. H. B. Temam and E. G. Temam, *Int. J. Electrochem. Sci*. 8 (2013) 914.
14. W. Lu, P. Huang, C. Z. He and B. Y. Arpn, *J. Eng. Appl. Sci*. 5 (2010) 6.
15. M. M. Abou-Krisha, *J Appl Surf Sci* 252 (2005) 1035.
16. A. G. Dolati, M. Ghorbani and A. Afshar, *Surf. Coat. Technol*. 166 (2003) 105.
17. T.V. Byk, T.V. Gaevskaya and L.S. Tsybulskaya, *Surf. Coat. Tech*. 202 (2008) 5817.
18. H. Y. Cheh and C. C. Wan, *J. Appl. Electrochem*. 3 (1973) 113.
19. M. M. Abou-Krisha, A. M. Zaky and A. A. Toghan, Morphology, *Asian Journal of Biochemistry* 1 (2006) 84.
20. M. J. Rahman, S. R. Sen, M. Moniruzzaman and K. M. Shorowordi, *J. Mech. Eng*. 40 (2009) 9.
21. A. C. Hegde, K. Venkatakrishna and N. Eliaz, *Surf. Coat. Technol*. 205 (2010) 2031.
22. N. Eliaz, K. Venkatakrishna and A. C. Hegde, *Surf. Coat. Technol*. 205 (2010) 1969.
23. J. Wu, Y. Jiang, C. Johnson and X. Liu, *J. Power Sources* 177 (2008) 376.